

---

This is an electronic reprint of the original article.  
This reprint may differ from the original in pagination and typographic detail.

Feng, Lin; Wang, Yibo; Sihvola, Ari; Qiu, Jinghui; Qi, Jiaran

## A Cross-Band Coupling Suppressed Tri-Band Base Station Array with Simultaneously Wideband Decoupling and Radiation Characteristics

*Published in:*  
IEEE Antennas and Wireless Propagation Letters

*DOI:*  
[10.1109/LAWP.2025.3632270](https://doi.org/10.1109/LAWP.2025.3632270)

E-pub ahead of print: 01/01/2025

*Document Version*  
Peer-reviewed accepted author manuscript, also known as Final accepted manuscript or Post-print

*Please cite the original version:*  
Feng, L., Wang, Y., Sihvola, A., Qiu, J., & Qi, J. (2025). A Cross-Band Coupling Suppressed Tri-Band Base Station Array with Simultaneously Wideband Decoupling and Radiation Characteristics. *IEEE Antennas and Wireless Propagation Letters*. Advance online publication. <https://doi.org/10.1109/LAWP.2025.3632270>

---

This material is protected by copyright and other intellectual property rights, and duplication or sale of all or part of any of the repository collections is not permitted, except that material may be duplicated by you for your research use or educational purposes in electronic or print form. You must obtain permission for any other use. Electronic or print copies may not be offered, whether for sale or otherwise to anyone who is not an authorised user.

# A Cross-Band Coupling Suppressed Tri-Band Base Station Array with Simultaneously Wideband Decoupling and Radiation Characteristics

Lin Feng, Yibo Wang, Ari Sihvola, *IEEE Life Fellow*, Jinghui Qiu, and Jiaran Qi, *Senior Member, IEEE*

**Abstract**—The simultaneous realization of wideband radiation and wideband cross-band decoupling in current 5G tri-band base station array remains a critical technical impediment. To address this challenge, a cross-band coupling suppressed tri-band base station antenna array based on radiative deep-subwavelength frequency selective surface (RFSS) with wideband decoupling and wideband radiation characteristics is proposed. The designed array consists of a low-band (LB) antenna operating in the range of 0.69–0.96 GHz (32.7%), a 2×2 middle-band (MB) antenna subarray operating in the range of 1.4–2.7 GHz (63.4%), and a 4×4 high-band (HB) antenna array operating in the range of 3.3–3.8 GHz (14.1%). In this configuration, the LB and MB antennas improve the radiation pattern distortions in 1.4–3.8 GHz (92.3%, which covers the bandwidth of MB and HB) and 3.3–3.8 GHz, respectively. A prototype for proof of the tri-band array is fabricated and measured. Experimental results confirm that the tri-band array exhibits the capability to achieve cross-band decoupling within wideband operational bandwidths.

**Index Terms**—Tri-band antenna, wideband radiation, wideband transmission, radiative deep-subwavelength frequency selective surface (RFSS), cross-band decoupling, base station antenna.

## I. INTRODUCTION

THE commercialization of the fifth-generation (5G) has established tri-band multi-antenna arrays as an essential requirement for new 5G base station deployments [1]. Due to the trend of global base station integration, the frequency band that needs to be covered by the new 5G base station antenna expands significantly. Consequently, tri-band base station antennas with wideband characteristics have emerged as a prominent research focus.

However, the cross-band coupling occurs in tri-band induces radiation pattern distortion in antenna elements, significantly compromising base station performance. To address cross-band coupling challenges in base station antenna arrays, electromagnetic transparent antennas [2]–[5] are proposed for cross-band scattering suppression. Chokes [6]–

This work was funded by the Natural Science Foundation of China (NSFC) Projects under Grant 62571161 and 62271170, and National Key Laboratory of Laser Spatial Information Foundation LSI2025ZZKY03. (Corresponding author: Jiaran Qi, e-mail: qi.jiaran@hit.edu.cn).

Lin Feng, Yibo Wang, Jinghui Qiu and Jiaran Qi are with the Department of Microwave Engineering, Harbin Institute of Technology, Harbin, 150001, China. (e-mail: qi.jiaran@hit.edu.cn).

Ari Sihvola is with the Department of Electronics and Nanoengineering, Aalto University, 00076 Espoo, Finland.

TABLE I  
COMPARISON WITH THE RELATED TRI-BAND DECOUPLING ARRAYS

Ref.	Decoupling Structure	LB OBW (GHz)	MB OBW (GHz)	HB OBW (GHz)	LB TBW / RBW(GHz)
[1]	SSR unit cells	0.79-0.96 (19.4%)	1.71-2.17 (23.7%)	VSWR<1.5 3.40-3.60 (5.7%)	–
[13]	Cascade comb-shaped	0.76-0.88 (14.6%)	1.90-2.70 (34.8%)	3.30-3.90 (16.7%)	–
[16]	–	–	1.43-1.52 (6.1%) & 1.92-2.18 (12.7%)	3.30-3.80 (14.1%)	–
[23]	FSS	0.69-0.96 (32.7%)	1.80-2.70 (40.0%)	3.30-3.80 (14.1%)	1.80-3.80 (71.4%)
[27]	FSS unit cells	–	RC<–15dB 1.70-2.70 (45.5%)	RC<–15dB HB1: 3.30-3.8 (14.1%) HB2: 4.80-5.00 (4.1%)	RC<–15dB 3.30-3.80 (14.1%) / 4.80-5.00 (4.1%)
[28]	FSS unit cells	–	1.60-2.70 (50.4%)	3.28-3.80 (14.9%) & 4.75-5.18 (8.6%)	3.28-3.80 (14.9%) & 4.75-5.18 (8.6%)
[29]	FSS unit cell	–	1.85-2.15 (15%)	HB1: 3.40-3.60 (5.7%) HB2: 5.40-5.60 (3.6%)	3.40-3.60 (5.7%) & 5.40-5.60 (3.6%)
Pro.	<b>RFSS</b>	<b>0.69-0.96 (32.7%)</b>	<b>1.40-2.70 (63.4%)</b>	<b>3.30-3.80 (14.1%)</b>	<b>1.40-3.80 (92.3%)</b>

OBW: Operating Bandwidth. TBW: Transmission Bandwidth. RBW: Reflection Bandwidth. RC: Reflection Coefficient.

[10] have been implemented for decoupling enhancement. Various shaped strips or branches [11]–[13] are integrated on the low-band (LB) radiator to suppress cross-band decoupling. A novel low-scattering antenna is proposed in [14] by discretizing solid metal into metal atoms and strategically connecting them to suppress strong scattering and mutual coupling. A filtered bowl-shaped LB antenna with helical filters integrated into radiators and LC circuits integrated into balun is designed in [15] to realize wideband decoupling. In [16], a tri-band base station antenna with low cross-band scattering characteristics is achieved through a stacked configuration. Besides, reactive loadings [17], metasurface [18]–[20], and partially reflecting surfaces [21] techniques have been employed to facilitate cross-band decoupling. In addition, frequency selective surface (FSS) has emerged as the commonly employed decoupling mechanism [22]–[29]. In [22] and [23], FSSs are inserted between antennas operating in different frequency bands to achieve decoupling. In [24], the

> REPLACE THIS LINE WITH YOUR MANUSCRIPT ID NUMBER (DOUBLE-CLICK HERE TO EDIT) <

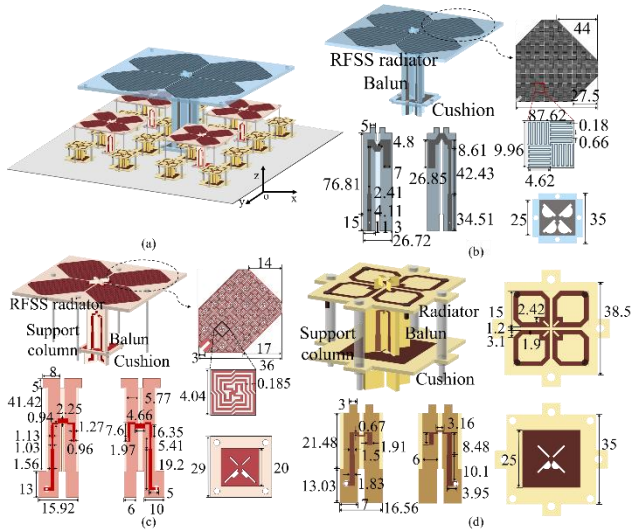


**Fig. 1.** Configuration of the proposed tri-band antenna array. (a) Tri-band array. (b) LB antenna element. (c) MB antenna element. (d) HB antenna element. (Units: mm.)

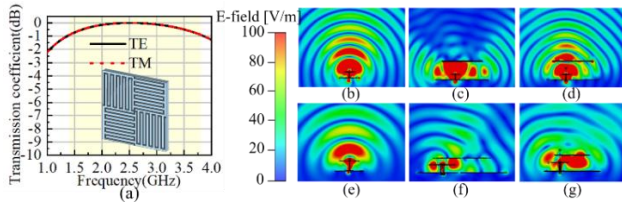


**Fig. 2.** (a) Transmission coefficient of the FSS unit cell.  $E$ -field distributions of the HB and MB antenna elements in  $yoz$ -plane. (b) Isolated HB antenna at 3.5 GHz. (c) HB antenna + conventional LB radiator at 3.5 GHz. (d) HB antenna + RFSS-based LB radiator at 3.5 GHz. (e) Isolated MB antenna at 2.0 GHz. (f) MB antenna + conventional LB radiator at 2.0 GHz. (g) MB antenna + RFSS-based LB radiator at 2.0 GHz.

LB antenna composed of a  $6 \times 6$  FSS array serves as a reflector for the high-band (HB) antenna elements positioned above. A two-layer FSS serves as an LB radiator to reduce its blockage on the HB elements located beneath in [25]. In [26]-[29], FSS unit cells are employed. However, the approaches above have yet to achieve wideband decoupling in tri-band arrays.

In this letter, a cross-band coupling suppressed tri-band base station array based on radiative deep-subwavelength frequency selective surface (RFSS) is designed. Although the RFSS method has been firstly proposed in previous published articles by the author in [30], however, compared with [30], this letter advances the prior framework by incorporating wideband decoupling characteristics alongside established wideband radiation performance, thereby extending dual-band to tri-band operational paradigms. The integration of RFSS enables simultaneously realization of wideband decoupling and wideband radiation within the proposed tri-band array.

## II. CONFIGURATION AND OPERATING MECHANISM OF THE TRI-BAND ANTENNA ARRAY

### A. Configuration of the Tri-band Antenna Array

The proposed tri-band antenna array, depicted in Fig. 1(a), incorporates a LB antenna, a  $2 \times 2$  middle-band (MB) subarray, and a  $4 \times 4$  HB subarray. The LB and MB antenna are designed

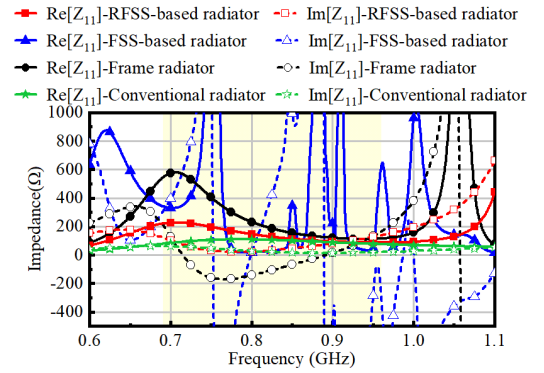


**Fig. 3** The impedance characteristics of four distinct radiator

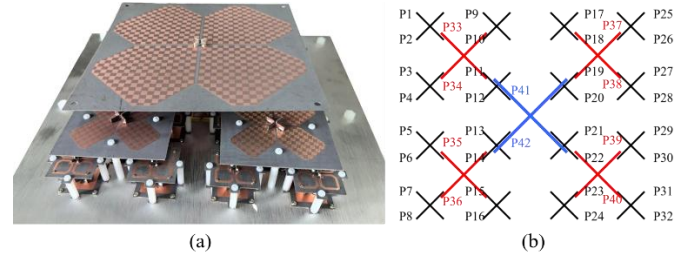


**Fig. 4** Prototype of the proposed tri-band array. (a) 3-D view. (b) Port labels.

to exhibit decoupling within respective bands — LB achieving decoupling for both MB and HB, and MB attains decoupling for HB. The structure of LB antenna element is shown in Fig. 1(b). The substrate of the LB radiator adopts F4B ( $\epsilon_r = 2.2$ ,  $\tan\delta = 0.001$ ) with a thickness of 0.8 mm. Approximately 232 FSS unit cells are etched on the radiator, with the unit size of  $9.96 \text{ mm} \times 9.96 \text{ mm} \times 0.8 \text{ mm}$  ( $0.086 \lambda_0 \times 0.086 \lambda_0 \times 0.0069 \lambda_0$  at 2.6 GHz). The balun utilizes F4B with a thickness of 1.5 mm. The cushion adopts FR-4 with a thickness of 0.8 mm. The MB antenna element incorporates the antenna architectural configuration reported in [30]. Dimensional modifications are implemented to optimize the performance within the tri-band array configuration as shown in Fig. 1(c). The structure of HB antenna element is shown in Fig. 1(d). All dielectric substrates are fabricated from F4B ( $\epsilon_r = 3.5$ ,  $\tan\delta = 0.001$ ) with a thickness of 0.8 mm.

### B. Decoupling Mechanism of the LB Antenna Element

The radiation characteristics of the MB antenna elements operating within 1.4-2.7 GHz, along with the transmission properties for electromagnetic waves in the HB band, have been comprehensively analyzed in the prior paper, consequently, this letter primarily examines the operational mechanism of the LB antenna. Firstly, the decoupling mechanism of LB antenna element for MB and HB is analyzed. Fig. 2(a) demonstrates that the deep-subwavelength FSS unit cell achieves transmission coefficients exceeding  $-1$  dB throughout 1.4-3.8 GHz (encompassing both MB and HB). The compact, meandering topological within the FSS structure ensures current paths corresponding to distinct resonant frequency points, thereby achieving the observed wideband characteristics. Fig. 2(b) - (f) delineates the  $E$ -field distributions across three distinct operational scenarios: the

> REPLACE THIS LINE WITH YOUR MANUSCRIPT ID NUMBER (DOUBLE-CLICK HERE TO EDIT) <

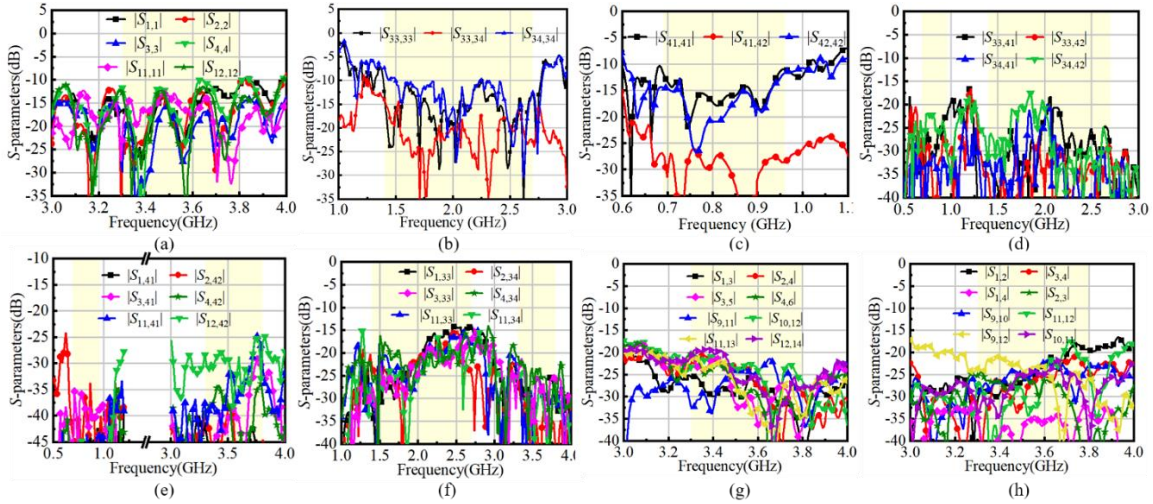


**Fig. 5.** The  $S$ -parameter measurement results of the tri-band base station antenna. (a) Reflection coefficient of the HB antenna elements. (b) Reflection coefficient and coupling coefficient of the MB antenna elements. (c) Reflection coefficient and coupling coefficient of the LB antenna elements. (d) Coupling coefficient of LB and MB antenna elements. (e) Co-polarization coupling coefficient of LB and HB antenna elements. (f) Co-polarization coupling coefficient of MB and HB antenna elements. (g) Co-polarization coupling coefficient of the HB antenna elements. (h) Cross-polarization coupling coefficient of HB antenna elements.

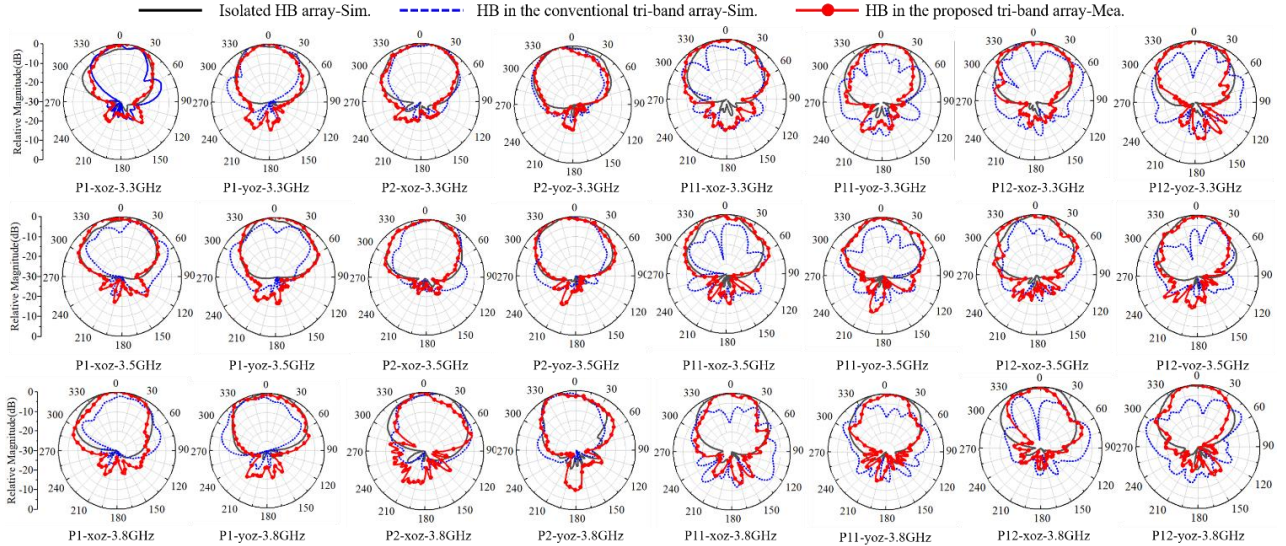


**Fig. 6.** Simulated and measured radiation patterns when port 1, port 2, port 11 and port 12 are excited, respectively.

isolated HB/MB antenna element, the HB/MB element beneath conventional LB radiator, and the HB/MB element beneath the proposed LB RFSS-based radiator. The conventional radiator maintains identical structural parameters to the proposed RFSS-based design, with the critical distinction residing in their dipole architectures, the RFSS implementation features a dipole structure integrating a deep-subwavelength FSS circumscribed by a narrow frame, whereas the conventional configuration employs a fundamental dipole topology. Comparative analysis reveals obvious  $E$ -field distortion in HB/MB elements beneath conventional LB radiators, whereas LB RFSS-based radiators mitigate distorted fields, restoring the field distributions to a state relatively consistent with those of isolated elements.

### C. Radiation Mechanism of the LB Antenna Element

The LB RFSS-based radiator integrates an FSS-based radiator and a narrow frame. To elucidate the radiation

mechanisms, comparative impedance analyses are conducted across four distinct radiator configurations: an RFSS-based LB radiator, a deep-subwavelength FSS-based radiator, a conventional radiator and a frame radiator. As shown in Fig. 3, the deep-subwavelength FSS-based radiator exhibit pronounced and erratic impedance oscillations, rendering effective impedance matching unattainable. Referring to the working mechanism of conventional radiators, a narrow frame is incorporated along the contour to form the RFSS-based radiator. The impedance characteristics of RFSS-based radiator exhibits both real and imaginary parts confined within an optimal operational range, which becomes more approximate to that of conventional radiators. Although the frame radiator exhibits comparatively stabilized impedance characteristics, the substantial magnitude of its real component within 0.69-0.80 GHz presents significant constraints on wideband impedance matching optimization.

> REPLACE THIS LINE WITH YOUR MANUSCRIPT ID NUMBER (DOUBLE-CLICK HERE TO EDIT) <

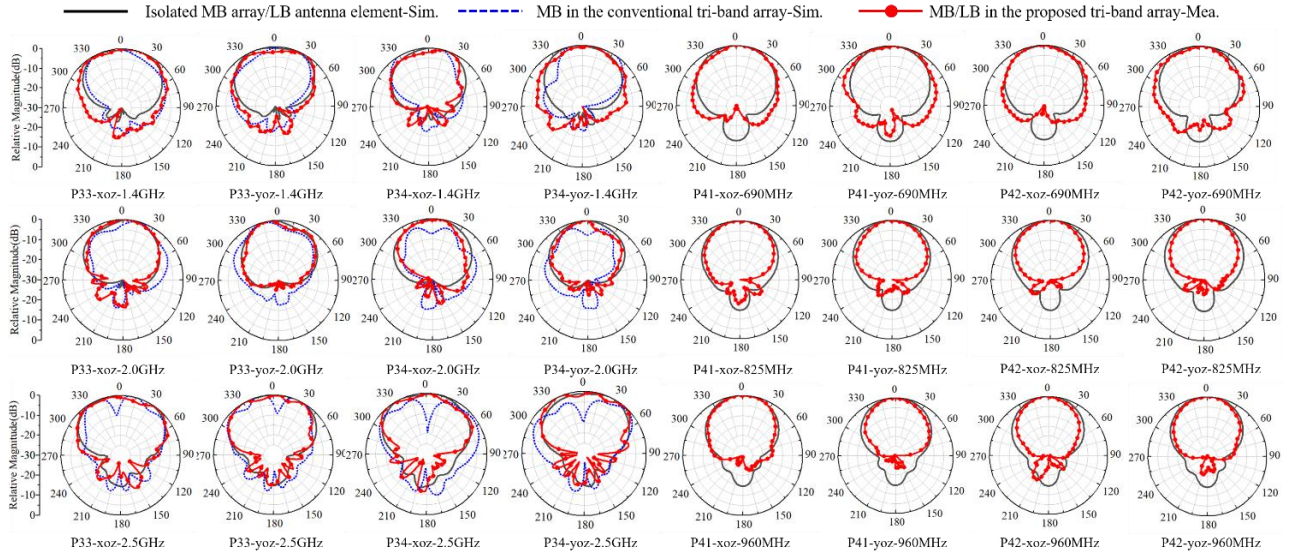


Fig. 7. Simulated and measured radiation patterns when port 33, port 34, port 41 and port 42 are excited, respectively.

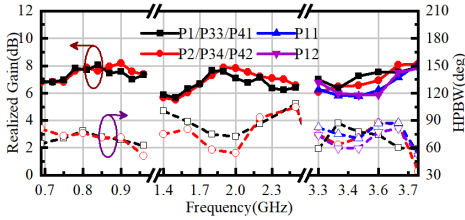


Fig. 8. Measured realized gain and HPBW of the tri-band antenna array.

### III. IMPLEMENTATION

#### A. Simulated and Measured Results

The proposed tri-band base station antenna is fabricated and measured, and the photograph of the antenna array is shown in Fig. 4(a). Fig. 4(b) delineates the antenna port configuration schema. Considering the structural symmetry of the array, experimental validation for MB is confined to P33-P34, while HB analysis focuses exclusively on ports P1, P2, P11 and P12.

As depicted in Fig. 5, the impedance bandwidths of the HB, MB and LB antenna elements encompass 3.3-3.8 GHz, 1.4-2.7 GHz and 0.69–0.96 GHz, respectively, with the reflection coefficient remaining below  $-10$  dB. The cross-band isolation between MB and LB antenna elements exceed 20 dB within LB and 17 dB within MB. The cross-band co-polarization isolation between LB and HB antenna elements exceeds 25 dB across both LB and HB. The cross-band co-polarization isolation between MB and HB antenna elements exceed 15 dB and 20 dB within MB and HB. Both the co-polarization and cross-polarization isolation between HB elements exceed 18 dB. In Fig. 6 and 7, the black curve represents the simulated radiation patterns of the antenna elements in the isolated HB/MB/LB array (without antenna elements operating in other frequency bands), the blue dashed line represents the simulated radiation patterns of the HB/MB antenna elements proposed in the conventional tri-band array (without any decoupling structures), and the red dotted line represents the measured radiation pattern of the HB/MB/LB antenna elements in the proposed RFSS-based decoupled tri-band array. From the results in Fig. 6, comparing the blue dashed line

and the black line, the antenna element with ports labeled P11 and P12 located at the center of the array have particularly severe distortion in the radiation patterns in the conventional array. Antenna element corresponding to edge-positioned ports P1 and P2 still exhibit radiation pattern distortions. Compared with the blue curve, by loading the RFSS structure, the red dotted line significantly alleviates the distortion of the radiation patterns. A comparable conclusion emerges from a comparison of the radiation patterns of P33 and P34 depicted in Fig. 7. At the boresight direction, the cross-polarization discrimination (XPD) of HB, MB, and LB antenna elements are greater than 14.5, 13, and 15.2 dB, respectively. Fig. 8 shows the measured realized gain and HPBW of the antenna elements in the tri-band array.

#### B. Comparison

Table I compares this work with the previous tri-band decoupled antenna arrays. Existing FSS-based decoupling methods typically employ approximately 4 FSS unit cells of conventional dimensions onto the radiators or insert FSS between antenna elements of different frequency bands for decoupling. Different from the aforementioned approaches, by integrating approximately 232 FSS unit cells with deep-subwavelength dimensions onto the LB radiator, periodicity is maximized — thereby ensuring the wideband decoupling capability. Simultaneously, the incorporation of narrow frame, together with FSS, form the RFSS configuration, collectively enables radiation.

### IV. CONCLUSION

In this letter, a tri-band base station antenna array based on RFSS cross-band decoupling method with wideband decoupling and wideband radiation characteristics is proposed. To achieve wideband decoupling, a deep-subwavelength FSS with transmission bandwidth of 92.3% is utilized. The optimized tri-band array demonstrates operational coverage spanning the LB from 0.69 to 0.96 GHz (32.7%), the MB from 1.4 to 2.7 GHz (63.4%), and the HB from 3.3 to 3.8 GHz (14.1%).

## REFERENCES

- [1] Y. -L. Chang and Q. -X. Chu, "Suppression of Cross-Band Coupling interference in tri-band shared-aperture base station antenna," *IEEE Trans. Antennas Propag.*, vol. 70, no. 6, pp. 4200-4214, June 2022.
- [2] Y. -L. Chang and Q. -X. Chu, "Broadband dual-polarized electromagnetic transparent antenna for cross-band scattering suppression," *IEEE Antennas Wireless Propag. Lett.*, vol. 21, no. 7, pp. 1452-1456, July 2022.
- [3] Y. -S. Wu, Q. -X. Chu and H. -Y. Huang, "Electromagnetic transparent antenna with slot-loaded patch dipoles in dual-band array," *IEEE Trans. Antennas Propag.*, vol. 70, no. 9, pp. 7989-7998, Sept. 2022.
- [4] R. C. Dai, H. Su, S. J. Yang, J. -H. Ou and X. Y. Zhang, "Broadband electromagnetic-transparent antenna and its application to aperture-shared dual-band base station array," *IEEE Trans. Antennas Propag.*, vol. 71, no. 1, pp. 180-189, Jan. 2023.
- [5] X. Zhang et al., "A novel broadband electromagnetic transparent structure and its application in dual-band aperture-shared base station antenna," *IEEE Antennas Wireless Propag. Lett.*, vol. 24, no. 7, pp. 1694-1698, July 2025.
- [6] H. -H. Sun, C. Ding, H. Zhu, B. Jones and Y. J. Guo, "Suppression of cross-band scattering in multiband antenna arrays," *IEEE Trans. Antennas Propag.*, vol. 67, no. 4, pp. 2379-2389, April 2019.
- [7] H. -H. Sun, C. Ding, H. Zhu, B. Jones and Y. J. Guo, "Suppression of cross-band scattering in multiband antenna arrays," *IEEE Trans. Antennas Propag.*, vol. 67, no. 4, pp. 2379-2389, April 2019.
- [8] R. Li, Y. Zhang, B. Xiao and Y. Cui, "An aperture-shared dual-band antenna array based on upstanding dipoles," *IEEE Antennas Wireless Propag. Lett.*, vol. 22, no. 11, pp. 2675-2679, Nov. 2023.
- [9] W. Yu, H. Lin, B. Liao and W. Duan, "A compact dual-polarized low-pass filtering antenna with wideband out-of-band rejection," *IEEE Antennas Wireless Propag. Lett.*, vol. 20, no. 12, pp. 2329-2333, Dec. 2021.
- [10] J. Jiang and Q. -X. Chu, "Dual-band shared-aperture base station antenna array based on 3-D chokes," *IEEE Antennas Wireless Propag. Lett.*, vol. 22, no. 4, pp. 824-828, April 2023.
- [11] Z. Chen, T. Xu, J. -F. Li, L. H. Ye and D. -L. Wu, "Dual-broadband dual-polarized base station antenna array with stable radiation pattern," *IEEE Antennas Wireless Propag. Lett.*, vol. 22, no. 2, pp. 303-307, Feb. 2023.
- [12] C. Liang, W. Yang, Q. Xue, W. Che and H. Wong, "Wideband high-transparent dipole antenna based on frequency selective surface and its applications in dual-band shared-aperture array," *IEEE Antennas Wireless Propag. Lett.*, vol. 24, no. 3, pp. 572-576, March 2025.
- [13] X. Lu, Y. Chen, S. Guo and S. Yang, "An electromagnetic-transparent cascade comb dipole antenna for multi-band shared-aperture base station antenna array," *IEEE Trans. Antennas Propag.*, vol. 70, no. 4, pp. 2750-2759, April 2022.
- [14] Y. Zhang and X. Chen, "Design of Shared-Aperture Multi-Band MIMO Antenna Array by Scattering Minimization," *IEEE Trans. Antennas Propag.*, doi: 10.1109/TAP.2025.3593977.
- [15] Y. He, C. Ding, C. Chang, G. Wei and Y. J. Guo, "A Bowl-Shaped Filtering Antenna with Wideband Cross-Band Scattering Mitigation for Dual-Band Base Stations," *IEEE Trans. Antennas Propag.*, vol. 72, no. 8, pp. 6723-6728, Aug. 2024.
- [16] Y. Li, W. Yang, Q. Xue and W. Che, "A miniaturized dual-polarized tri-band antenna based on multimode and stacked scheme for multiband aperture-shared base-station applications," *IEEE Trans. Antennas Propag.*, vol. 72, no. 5, pp. 4647-4652, May 2024.
- [17] M. Li, M. Y. Jamal, C. Zhou, L. Jiang and L. K. Yeung, "A novel dipole configuration with improved out-of-band rejection and its applications in low-profile dual-band dual-polarized stacked antenna arrays," *IEEE Trans. Antennas Propag.*, vol. 69, no. 6, pp. 3517-3522, June 2021.
- [18] F. Du, Y. Cao, X. Xiu, W. Che and Q. Xue, "Compact dual-band shared-aperture base-station antenna array using transparent wideband absorbing metasurface and radiator-reused scheme," *IEEE Trans. Antennas Propag.*, vol. 72, no. 3, pp. 2502-2512, March 2024.
- [19] P. Du, Y. Cao, W. Che and Q. Xue, "Low-profile dual-band dual-polarized aperture-shared antenna array using bifunctional metasurface," *IEEE Trans. Antennas Propag.*, vol. 73, no. 7, pp. 4274-4285, July 2025.
- [20] Y. F. Cao, X. Y. Zhang and Q. Xue, "Compact shared-aperture dual-band dual-polarized array using filtering slot antenna and dual-function metasurface," *IEEE Trans. Antennas Propag.*, vol. 70, no. 2, pp. 1120-1131, Feb. 2022.
- [21] Y. Qin, R. Li, Q. Xue, X. Zhang and Y. Cui, "Aperture-shared dual-band antennas with partially reflecting surfaces for base-station applications," *IEEE Trans. Antennas Propag.*, vol. 70, no. 5, pp. 3195-3207, May 2022.
- [22] Y. Zhu, Y. Chen and S. Yang, "Cross-band mutual coupling reduction in dual-band base-station antennas with a novel grid frequency selective surface," *IEEE Trans. Antennas Propag.*, vol. 69, no. 12, pp. 8991-8996, Dec. 2021.
- [23] D. He, Y. Chen and S. Yang, "A low-profile triple-band shared-aperture antenna array for 5G base station applications," *IEEE Trans. Antennas Propag.*, vol. 70, no. 4, pp. 2732-2739, April 2022.
- [24] H. Li, J. Xu, Y. Nan, Q. Chen and C. Zhou, "Low-profile dual-band shared-aperture base station antennas based on FSS radiators," *IEEE Antennas Wireless Propag. Lett.*, vol. 23, no. 6, pp. 1894-1898, June 2024.
- [25] S. J. Yang and X. Y. Zhang, "Frequency selective surface-based dual-band dual-polarized high-gain antenna," *IEEE Trans. Antennas Propag.*, vol. 70, no. 3, pp. 1663-1671, March 2022.
- [26] D. He, Q. Yu, Y. Chen and S. Yang, "Dual-band shared-aperture base station antenna array with electromagnetic transparent antenna elements," *IEEE Trans. Antennas Propag.*, vol. 69, no. 9, pp. 5596-5606, Sept. 2021.
- [27] J. -X. Chen, X. -F. Wang, L. -L. Yang, X. -R. Wang, X. -F. Gu and W. -W. Yang, "Asymmetrical low-RCS FSS-based antenna for tri-band shared-aperture array," *IEEE Antennas Wireless Propag. Lett.*, vol. 23, no. 5, pp. 1563-1567, May 2024.
- [28] G. -N. Zhou, B. -H. Sun, Q. -Y. Liang, S. -T. Wu, Y. -H. Yang and Y. -M. Cai, "Triband dual-polarized shared-aperture antenna for 2G/3G/4G/5G base station applications," *IEEE Trans. Antennas Propag.*, vol. 69, no. 1, pp. 97-108, Jan. 2021.
- [29] Y. Sun, J. Zhang, P. Mei, S. Luo, W. Fu and S. Zhang, "Tri-band dual-polarized shared-aperture antenna arrays with wide-angle scanning and low profile for 5G base stations," *IEEE Trans. Antennas Propag.*, vol. 72, no. 3, pp. 2455-2467, March 2024.
- [30] L. Feng et al., "Radiative deep-subwavelength frequency-selective surface-based cross-band decoupling method for base station antenna," *IEEE Trans. Antennas Propag.*, vol. 73, no. 2, pp. 771-781, Feb. 2025.